Phenylboronic Acid-Decorated Chondroitin Sulfate A-Based Theranostic Nanoparticles for Enhanced Tumor Targeting and Penetration

Jae-Young Lee, Suk-Jae Chung, Hyun-Jong Cho, and Dae-Duk Kim**

Phenylboronic acid-functionalized chondroitin sulfate A (CSA)–deoxycholic-acid (DOCA)-based nanoparticles (NPs) are prepared for tumor targeting and penetration. (3-Aminomethylphenyl)boronic acid (AMPB) is conjugated to CSA–DOCA conjugate via amide bond formation, and its successful synthesis is confirmed using proton nuclear magnetic resonance spectroscopy (^{1}H-NMR). Doxorubicin (DOX)-loaded CSA–DOCA–AMPB NPs with a mean diameter of ≈200 nm, a narrow size distribution, negative zeta potential, and spherical morphology are prepared. DOX release from NPs is enhanced at acidic pH compared to physiological pH. CSA–DOCA–AMPB NPs exhibit improved cellular uptake in A549 (human lung adenocarcinoma) cells and penetration into A549 multicellular spheroids compared to CSA–DOCA NPs as evidenced by confocal laser scanning microscopy and flow cytometry. In vivo tumor targeting and penetrating by CSA–DOCA–AMPB NPs, based on both CSA–CD44 receptor and boronic acid–sialic acid interactions, is revealed using near-infrared fluorescence (NIRF) imaging. Penetration of NPs to the core of the tumor mass is observed in an A549 tumor xenografted mouse model and verified by three-dimensional NIRF imaging. Multiple intravenous injections of DOX-loaded CSA–DOCA–AMPB NPs efficiently inhibit the growth of A549 tumor in the xenografted mouse model and increase apoptosis. These boronic acid-rich NPs are promising candidates for cancer therapy and imaging.

1. Introduction

The selective delivery of high doses of drug to tumors is regarded as the main objective of cancer chemotherapy. The enhanced permeability and retention (EPR) effect can be adopted as a passive tumor targeting strategy and is based on the aberrant vasculature of tumors that results from angiogenesis and an immature lymphatic system.[1] If nanocarriers have suitable physicochemical properties (i.e., particle size, shape, and surface charge), the EPR effect causes them to accumulate in tumors.[2] However, passive tumor targeting based on the EPR effect provides unspecific tumor targeting; therefore, tumor-specific targeting moieties have been introduced to nanocarriers in order to enhance their selective tumor targeting. The conjugation of tumor-specific ligands (i.e., small molecules, peptides, and antibodies) that are able to interact with receptors overexpressed in cancer cells to nanocarriers is called an active tumor targeting strategy,[3–6] and has been widely used in conjunction with passive tumor targeting strategies.

Even though the use of the above mentioned tumor-targeting strategies can result in some anticancer activity, clinically effective therapeutics require homogenous distribution of therapeutic agents across the entire tumor, and this is not easily achieved. The delivery of drugs to solid tumors is hampered by their characteristic features such as increased stiffness of the tumor extracellular matrix (ECM) and high interstitial fluid pressure (IFP).[7,8] The abnormal ECM and high IFP in tumors can prevent the penetration of anticancer agents into the core of tumors. Successful distribution of anticancer drugs to the core of the tumor would allow the establishment of a fully effective cancer therapy and prevent metastasis and relapse. To overcome the stiff ECM and high IFP of solid tumors, there are several strategies that can be employed: the ECM can be degraded with enzymes (i.e., hyaluronidase and collagenase); tumor-targeting ligands can be introduced (i.e., folic acid); and agents that reduce IFP can be used (i.e., vasotargeting agents, vascular disrupting agents, vasodilators, and tumor growth factor-beta inhibitors).[9]

To aid tumor penetration, sialic acid-targeting strategy can be used to enhance intratumoral transport of nanocarriers.[10] It has been reported that sialylated epitopes (glycan chains including *N*-acetylneuraminic acid) are overexpressed on cancer cells, and their presence is implicated in metastasis, progression, apoptosis, and resistance to chemotherapy.[11,12] Phenylboronic acid can selectively recognize the sialic acid expressed on cancer cells and can therefore be used as a tumor-targeting

J.-Y. Lee, Prof. S.-J. Chung, Prof. D.-D. Kim
College of Pharmacy and Research Institute of Pharmaceutical Sciences
Seoul National University
Seoul 151-742, Republic of Korea
E-mail: ddkim@snu.ac.kr
Prof. H.-J. Cho
College of Pharmacy
Kangwon National University
Chuncheon 200-701, Republic of Korea
E-mail: hjcho@kangwon.ac.kr

DOI: 10.1002/adfm.201500680

moiety.[13–15] Complex formation between sialic acid and phenylboronic acid is favored because of the trigonal structure of boron.[12] Tumor targeting using phenylboronic acid has several advantages such as high binding affinity and selectivity, nontoxicity, nonimmunogenicity, and inexpensiveness.[12]

In this work, phenylboronic acid was conjugated to an amphiphilic chondroitin sulfate A–deoxycholic acid (CSA–DOCA) conjugate to form nanoparticles (NPs). It is known that CSA can bind to the CD44 receptor expressed in cancer cells.[16] NPs based on chondroitin sulfate derivatives have been used for tumor targeting and anticancer drug delivery.[17,18] Tumor targeting and penetrating strategies based on the interaction between CSA and CD44 receptor combined with the interaction between sialic acid and boronic acid are envisaged to increase the usefulness of NPs for selective drug delivery to tumors and result in homogeneous distribution across solid tumors. Along with an investigation of tumor targeting, the penetration of NPs into the tumor mass was investigated using in vitro and in vivo 3D tumor models.

2. Results and Discussion

2.1. Synthesis and Characterization of (3-Aminomethylphenyl)boronic Acid (AMPB)-Conjugated CSA–DOCA (CSA–DOCA–AMPB)

Figure 1 shows the schematic illustration of tumor targeting and penetrating strategy of doxorubicin (DOX)-loaded CSA–DOCA–AMPB NPs. Phenylboronic acid conjugated to CSA–DOCA to yield the CSA–DOCA–AMPB can interact with sialic acid on the surface of cancer cells to form boronate esters.[10,13] CSA–DOCA was successfully synthesized by conjugating ethylenediamine-modified DOCA (EtDOCA) to CSA through the formation of an amide bond (**Figure 2**A). To attach ethylenediamine to DOCA, the carboxylic acid group of DOCA was first converted to a methyl ester. The methoxy group was then replaced with an ethylenediamine linker via a nucleophilic substitution. The resultant product, EtDOCA, was conjugated to CSA using an 1-ethyl-3-(3-dimethylaminopropyl) carbodiimide (EDC) and *N*-hydroxysuccinimide (NHS)-mediated coupling reaction. The characteristic peaks of EtDOCA (0.6 ppm [C18 methyl group]; 2.5–3.0 ppm [ethylene group]; 7.8–8.0 ppm [amide group]) in the ^{1}H-NMR spectrum of the final product indicate successful synthesis of CSA–DOCA (Figure 2B). The degree of substitution (8.92%) of the EtDOCA group to CSA was calculated by comparing the integrations of shift "a" (1.8 ppm; *N*-acetyl group of CSA) and shift "b" (0.6 ppm; C18 methyl group of DOCA).

The attachment of phenylboronic acid groups to CSA–DOCA was achieved using AMPB. The AMPB has a primary amine group, which can react with the carboxylic acid group on CSA–DOCA through EDC/NHS-mediated amide bond formation. As shown in the ^{1}H-NMR spectrum of AMPB–CSA–DOCA (Figure 2B), the presence of signals representing the aromatic protons (d and e, 7.3–7.4 ppm; c and f, 7.6–7.7 ppm) of AMPB implies successful introduction of phenylboronic acid groups to CSA–DOCA. To calculate the AMPB content, a simple linear regression method with the ^{1}H-NMR spectra of

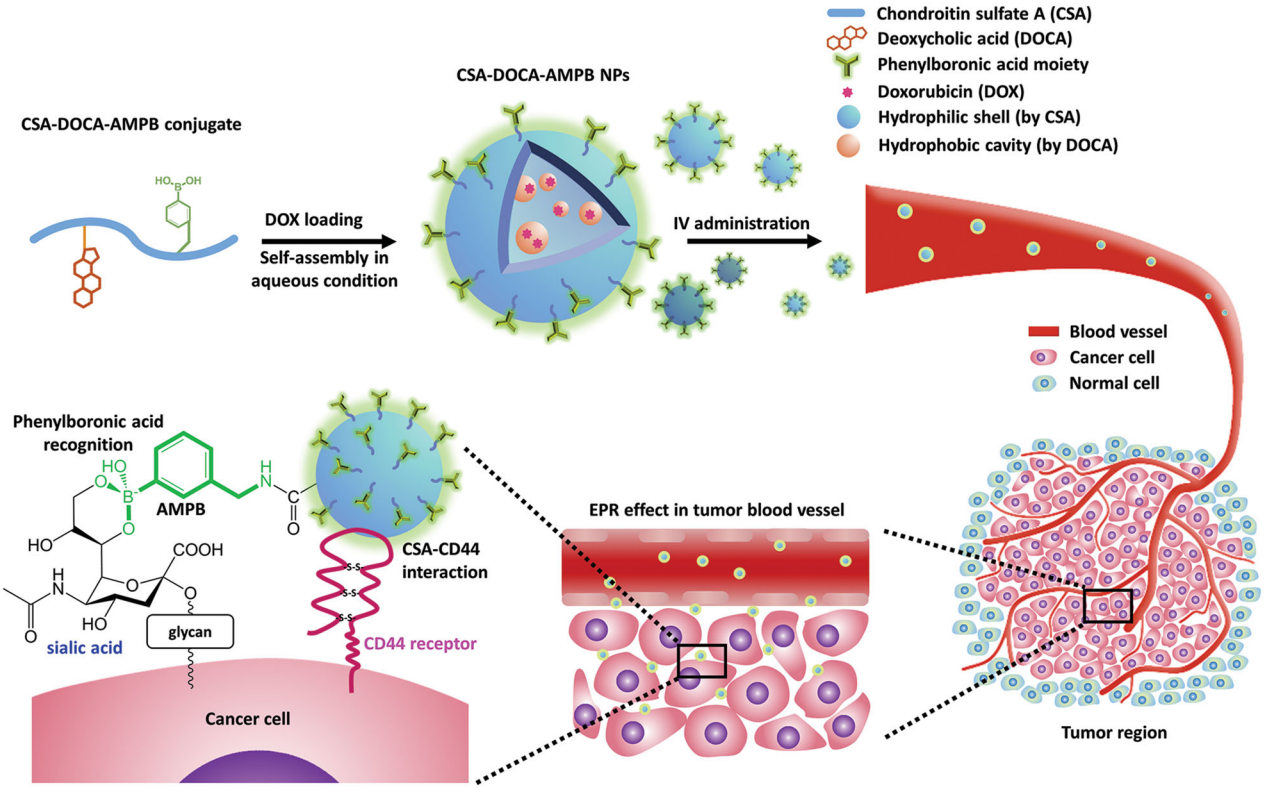

Figure 1. Schematic illustration about tumor targeting and penetrating action of CSA–DOCA–AMPB/DOX NPs.

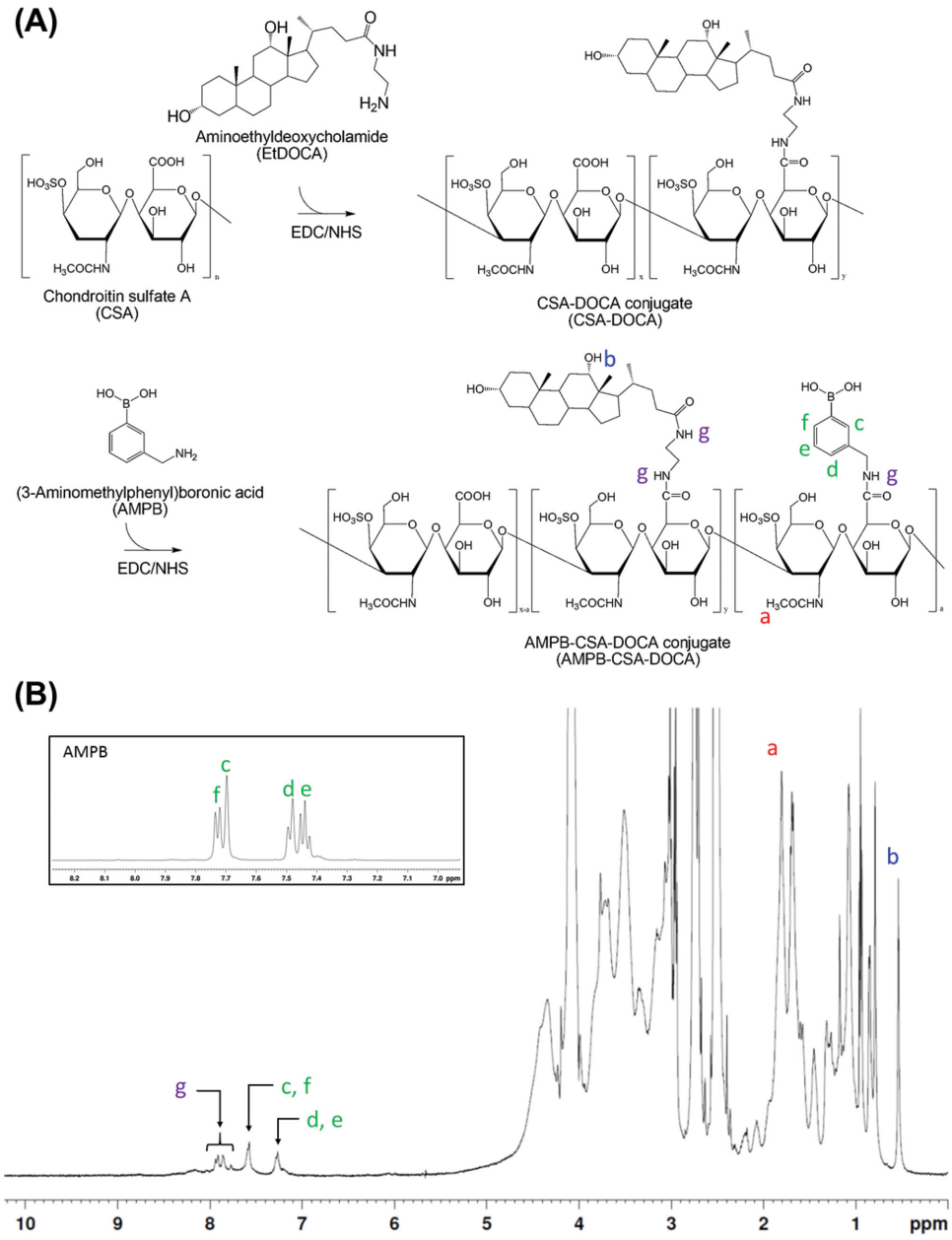

Figure 2. Synthesis and its verification of CSA–DOCA–AMPB conjugate. A) Scheme for the synthesis of CSA–DOCA–AMPB is presented. B) ^{1}H-NMR spectrum of CSA–DOCA–AMPB is shown. Inset indicates ^{1}H-NMR spectrum of AMPB. The chemical shifts for CSA (a, 1.8 ppm), EtDOCA (b, 0.6 ppm; g, 7.8–8.0 ppm), and AMPB (d,e, 7.3–7.4 ppm; c,f, 7.6–7.7 ppm) are shown in the spectrum of CSA–DOCA–AMPB. CSA–DOCA–AMPB was dissolved in the mixture of DMSO-d_6 and D_2O mixture (3:1, v/v) for ^{1}H-NMR (500 MHz) analysis.

AMPB/CSA–DOCA physical mixtures was used. Representative signals of AMPB (7.6–7.7 ppm) and CSA–DOCA (0.6 ppm; 3H from C18 methyl group of DOCA) were used to draw the regression line, whereby the *X*- and *Y*-axes represent the weight ratio and integration ratio of the peaks, respectively (data not shown). The content of introduced AMPB in CSA–DOCA–AMPB was 2.35% (w/w) according to the ^{1}H-NMR data (Figure 2).

It has been reported that the phenylboronic acid residue contains a fluorophore; thus, the extent of the conjugation of AMPB to CSA–DOCA was assessed by measuring fluorescence.[12] As shown in Figure S1 (Supporting Information), the maximum emission of AMPB was presented at 297 nm. CSA–DOCA has a lower peak emission at around 370 nm. These properties were reflected in the spectrum of CSA–DOCA–AMPB. The maximum fluorescence intensity of AMPB was the same as that of CSA–DOCA–AMPB (at a comparable concentration as calculated by ^{1}H-NMR analysis) at an emission wavelength of 297 nm. Interestingly, the linearity of the correlation between AMPB concentration and maximum fluorescence intensity was established across the whole concentration range tested (inset

Table 1. Characterization of developed DOX-loaded NPs.

Composition	Mean diameter [nm]	Polydispersity index	Zeta potential [mV]	Encapsulation efficiency [%][a)]
CSA–DOCA/DOX NPs	228.9 ± 2.0	0.22 ± 0.01	−22.58 ± 1.82	80.87 ± 0.18
CSA–DOCA–AMPB/DOX NPs	205.8 ± 8.2	0.21 ± 0.01	−20.97 ± 0.75	71.71 ± 0.24

[a)] Encapsulation efficiency (%) = $\frac{\text{actual amount of DOX in NPs}}{\text{input amount of DOX in NPs}} \times 100$

The weight ratio between polymer and drug was 7.5:1.
Data are presented as mean ± SD ($n = 3$).

of Figure S1, Supporting Information). This confirmed the successful attachment of AMPB molecules to the CSA–DOCA conjugate, as shown by ^{1}H-NMR analysis.

2.2. Preparation and Characterization of DOX-Loaded NPs

NPs based on CSA–DOCA or CSA–DOCA–AMPB were fabricated according to a previously reported solvent evaporation method.[19,20] DOX base was used as a model hydrophobic anticancer drug and was incorporated into CSA–DOCA and CSA–DOCA–AMPB NPs. CSA–DOCA is an amphiphile composed of a hydrophilic backbone (CSA) and hydrophobic pendant groups (DOCA). Thus, in an aqueous environment, CSA–DOCA may form NPs over its critical aggregation concentration. AMPB, a ligand for sialic acid overexpressed in cancer cells, was conjugated to the CSA backbone. After loading of DOX, the CSA–DOCA and CSA–DOCA–AMPB NPs exhibited a mean diameter of 206–229 nm, a narrow size distribution, negative zeta potential, and 70%–80% drug encapsulation efficiency (**Table 1** and **Figure 3**A). A spherical morphology was observed, and mean diameter was confirmed using transmission electron microscopy (TEM) imaging (Figure 3B). The particle size of the prepared CSA–DOCA–AMPB/DOX NPs was suitable for taking advantage of the EPR effect for the purpose of passive tumor targeting.[21] In previous reports, self-assembled NPs based on amphiphilic hyaluronic acid oligomer and chitosan oligosaccharide had a particle size of <200 nm and showed in vivo anticancer efficacy via tumor targeting.[19,20,22] Therefore, the CSA-based NPs discussed herein, which have similar physicochemical properties, are expected to also show tumor targeting and antitumor efficacy in vivo.

After intravenous injection, NPs may react with plasma proteins and form aggregates in the blood stream. Reaction with blood components will interfere with specific tumor-targeted delivery and result in the distribution of NPs to normal tissues and organs. To evaluate the in vitro stability of the prepared NPs in the biological fluids, the particle size of NPs in serum-containing media as well as phosphate buffered saline (PBS, pH 7.4) was monitored. As shown in Figure S2 (Supporting Information), the particle size and size distribution of DOX-loaded NPs were measured for 24 h. After incubation for 24 h in PBS (pH 7.4) and serum (50% FBS), the initial mean diameters of NPs were maintained. Particularly, the maintenance of initial particle size in serum may ensure efficient circulation of NPs in the blood stream.

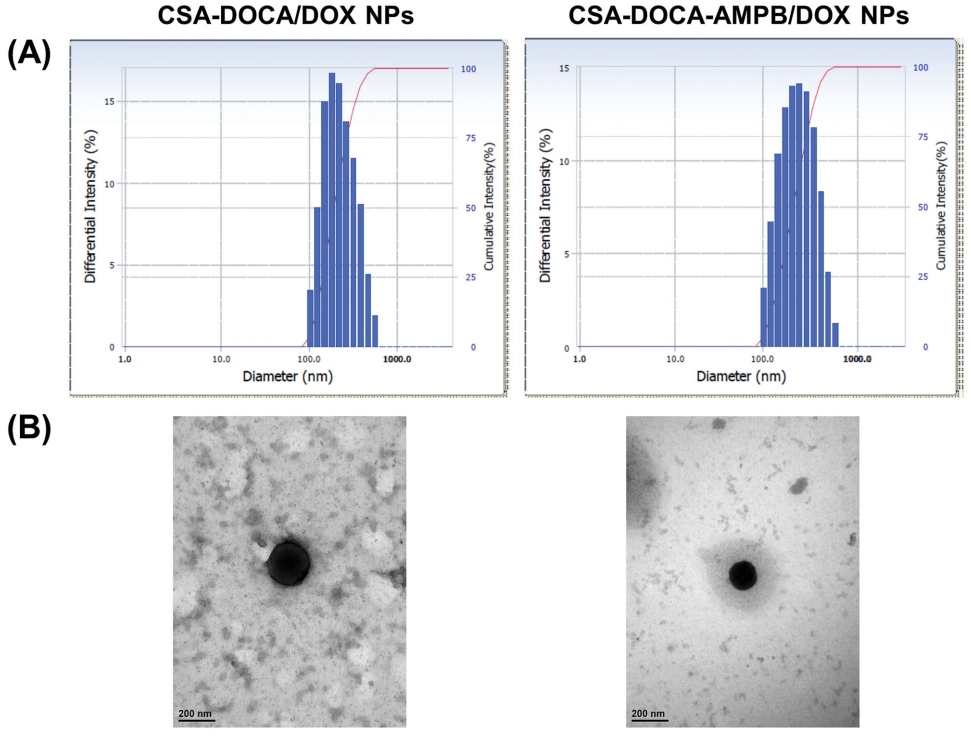

Figure 3. Characterization of CSA–DOCA/DOX NPs and CSA–DOCA–AMPB/DOX NPs. A) Size distribution, plotted as a differential intensity according to the mean diameter, of developed NPs is shown. B) TEM images of both NPs groups are presented. The length of the scale bar is 200 nm.

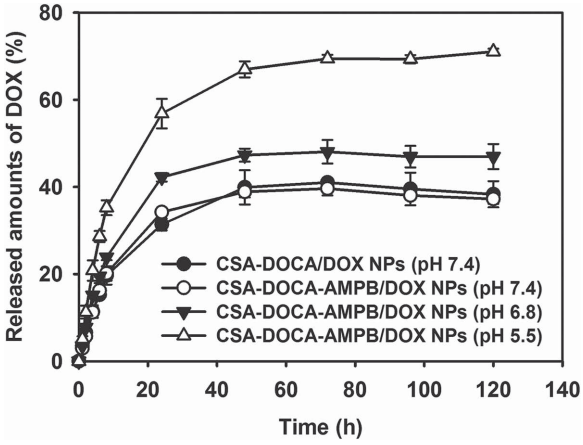

Figure 4. In vitro DOX release profiles from NPs. The released amounts of DOX (%), at pH 7.4, 6.8, and 5.5, are plotted to the incubation time. Each point represents the mean ± SD ($n = 3$).

2.3. In Vitro Drug Release

DOX release from the NPs was evaluated at different pH values. A sustained drug release pattern is a desirable characteristic of parenteral formulations. Compared to drug solutions, nanosized formulations generally exhibit a more sustained drug release profile and therefore allow a reduced dosing frequency and improved pharmacological efficacy. In our previous studies,[3,19,20,22,23] self-assembled NPs based on amphiphilic derivatives of hyaluronic acid oligomer and chitosan oligosaccharide exhibited a sustained release over several days. In this investigation, drug release was maintained for 5 days, and a sustained release profile was observed (**Figure 4**). There was no significant difference in the amount of drug released from CSA–DOCA NPs and CSA–DOCA–AMPB NPs at pH 7.4. AMPB decoration of CSA–DOCA NPs did not significantly influence their drug release pattern. Among the three pH values investigated (pH 5.5, 6.8, and 7.4), the highest amounts of DOX were released at pH 5.5. On day 5, the amount of DOX that was released at pH 5.5 was 1.91-fold higher than that at pH 7.4 (as a relative ratio). This may be related to the enhancement of DOX solubility and reduction of the interactions between drug and NP structure.[19] It should be noted that pH 5.5, 6.8, and 7.4 correspond to the pH of endocytic compartments (endosome and lysosome), the tumor microenvironment, and normal physiological conditions, respectively; therefore, improved drug release at an acidic pH (pH 5.5 and 6.8), compared to normal physiological pH (pH 7.4), is a desired characteristic of NPs for anticancer drug delivery. Higher drug release in cancer cells than in normal tissues and organs can lead to enhanced antitumor efficacy and reduce unwanted side effects.

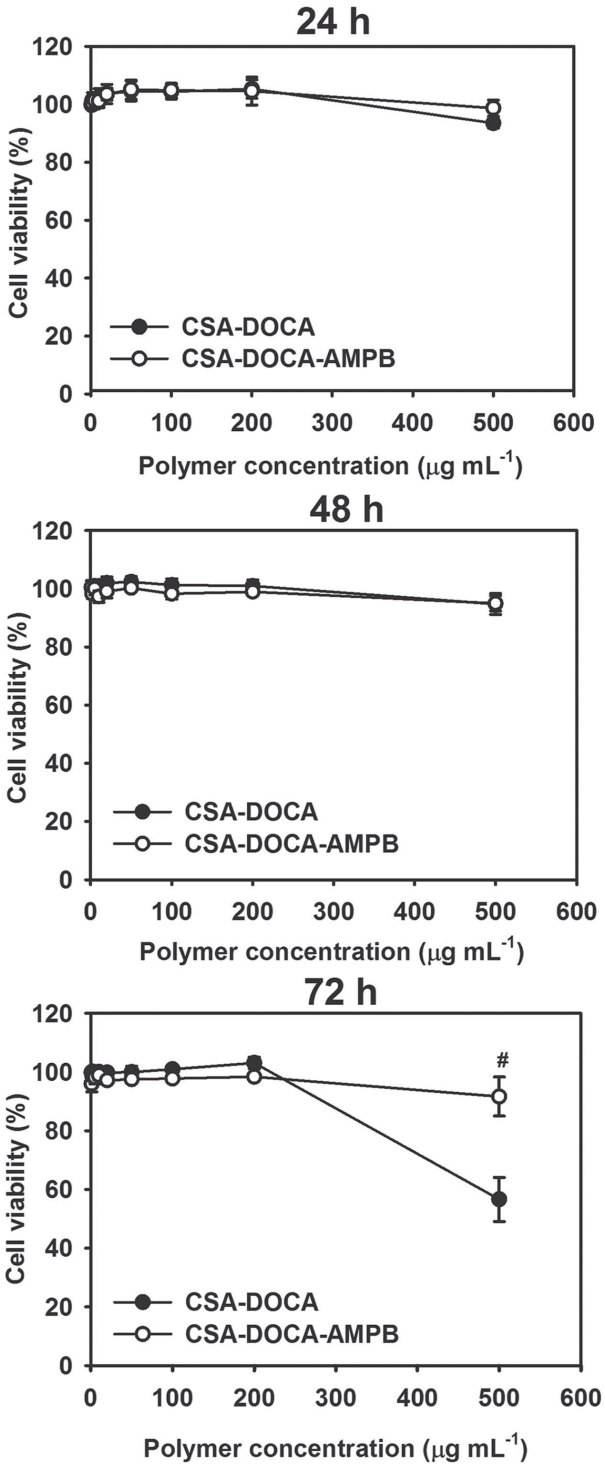

Figure 5. Cytotoxicity of CSA–DOCA and CSA–DOCA–AMPB in A549 cells. Cell viability (%) was determined by MTS-based assay at various polymer concentrations (≈500 μg mL^{-1}) after 24, 48, and 72 h of incubation. Each point represents the mean ± SD ($n = 6$). $^{\#}p < 0.05$, compared to CSA–DOCA group.

2.4. In Vitro Cytotoxicity

The cytotoxicity of the CSA–DOCA and CSA–DOCA–AMPB conjugates was assessed in A549 cells (**Figure 5**). A549 cells have been used as a CD44 receptor-positive cell line to assess the tumor-targeting ability of drug delivery systems incorporating ligands for that receptor.[24] After incubating for 24 and

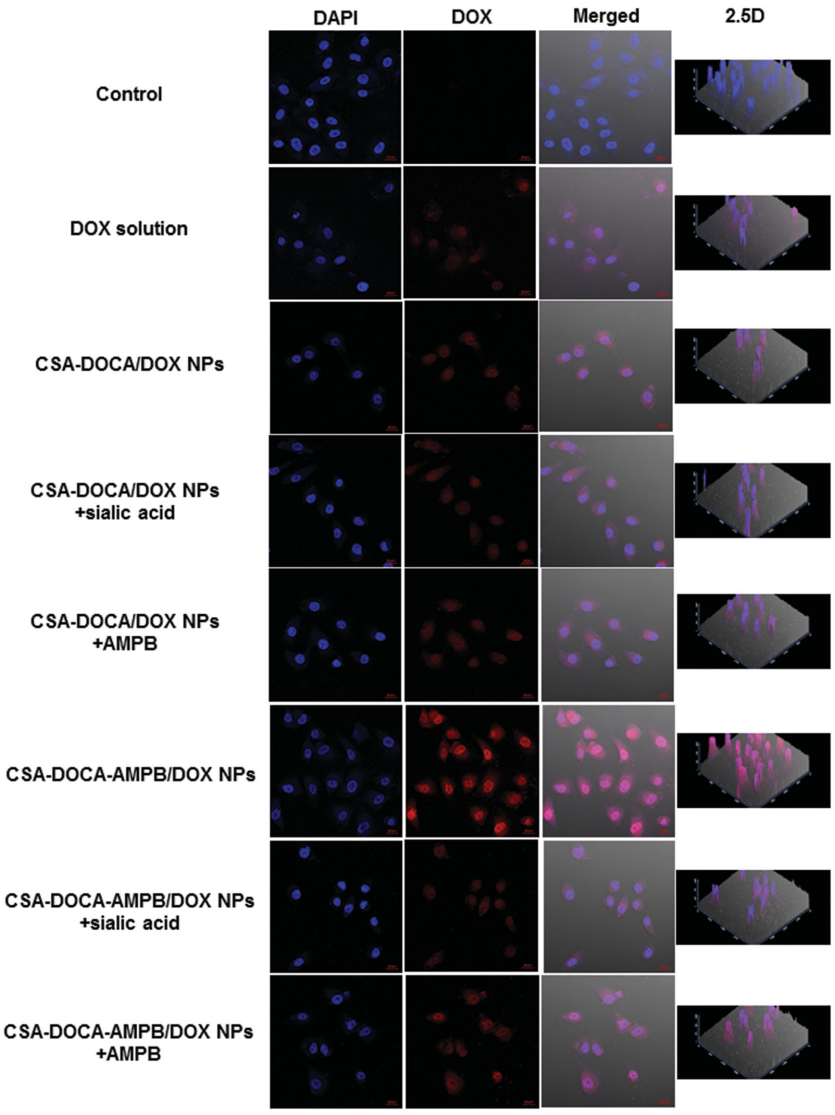

Figure 6. Cellular uptake study in A549 cells, cultured in 2D model, observed by CLSM. DOX solution, CSA–DOCA/DOX NPs, and CSA–DOCA–AMPB/DOX NPs (corresponded to 100×10^{-6} M of DOX) were incubated for 1 h in A549 cells. Sialic acid (500×10^{-6} M) was pre-incubated with NPs suspension before adding to the cultured cells. And AMPB (500×10^{-6} M) was preincubated with the cells prior to the treatment of NPs suspension. Blue and red color indicate DAPI and DOX, respectively. The length of bar (red) in the each image is 20 μm.

2.5. In Vitro Cellular Uptake and Antitumor Efficacy Test in 2D Cell Culture Model

The cellular distribution and efficiency of DOX uptake in A549 cells were assessed by confocal laser scanning microscopy (CLSM) and flow cytometry (**Figure 6** and Figure S3, Supporting Information). CD44 receptor-mediated endocytosis of chondroitin sulfate-based NPs has already been reported.[16] In our investigation, free sialic acid or boronic acid (as an AMPB) was added to verify the interaction between phenylboronic acid and sialic acid and to observe its influence on the cellular uptake of phenylboronic acid-decorated NPs. As shown in Figure 6 and Figure S3 (Supporting Information), the uptake of DOX increased in the following order; DOX solution, CSA–DOCA/DOX NPs, and CSA–DOCA–AMPB/DOX NPs. As previously reported,[22] DOX solution and DOX-loaded NPs have different uptake mechanisms: passive diffusion versus receptor-mediated endocytosis. Nonetheless, NPs group exhibited better cellular uptake efficiency rather than drug solution group due to receptor-mediated endocytosis. Also, considering the higher cellular uptake efficiency of DOX in CSA–DOCA–AMPB NPs group compared to CSA–DOCA NPs group ($p < 0.05$), phenylboronic acid–sialic acid interactions as well as CSA–CD44 receptor interactions seemed to significantly elevate the extent of drug uptake. The pretreatment of free sialic acid or free AMPB with CSA–DOCA–AMPB/DOX NPs group markedly reduced the drug cellular uptake ($p < 0.05$), comparable to that of the CSA–DOCA/DOX NPs group (Figure 6 and Figure S3, Supporting Information). Complex formation between free sialic acid and AMPB of NPs seemed to inhibit the binding of AMPB-NPs to the cancer cells. This confirms that the interaction between phenylboronic acid and sialic acid plays an important role in the cellular uptake of AMPB-modified NPs.

These cellular distribution and uptake efficiency of the developed AMPB-modified NPs were evaluated by in vitro MTS-based assay. As shown in Figure S4 and Table S1 (Supporting Information), cell viability profiles and IC_{50} values of DOX solution, CSA–DOCA/DOX NPs, and CSA–DOCA–AMPB/DOX NPs were acquired after 24, 48, and 72 h of incubation in A549 cells. In all groups, cell viability decreased as incubation period increased. In particular, the order of cytotoxicity, at 48 and 72 h incubation groups, was as follows: DOX solution < CSA–DOCA/DOX NPs < CSA–DOCA–AMPB/DOX NPs ($p < 0.05$). These results also implied the contribution of both CSA–CD44 receptor and phenylboronic acid–sialic acid interactions to the improved cellular uptake of CSA–DOCA–AMPB NPs.

48 h, neither conjugate had induced serious cytotoxicity at any of the concentrations tested (~500 μg mL^{-1}). However, after 72 h incubation, the cell viability of the CSA–DOCA-treated group decreased to about 56%, while that of CSA–DOCA–AMPB-treated group was around 92% ($p < 0.05$). Although the specific mechanism is not revealed yet, attachment of AMPB to CSA–DOCA seems to reduce cytotoxicity. Both components of CSA–DOCA are classified as biocompatible and both materials have been widely used for the fabrication of drug carriers.[25–28] The negligible cytotoxicity of CSA–DOCA–AMPB suggests that it can be safely used in injectable formulations for anticancer drug delivery.

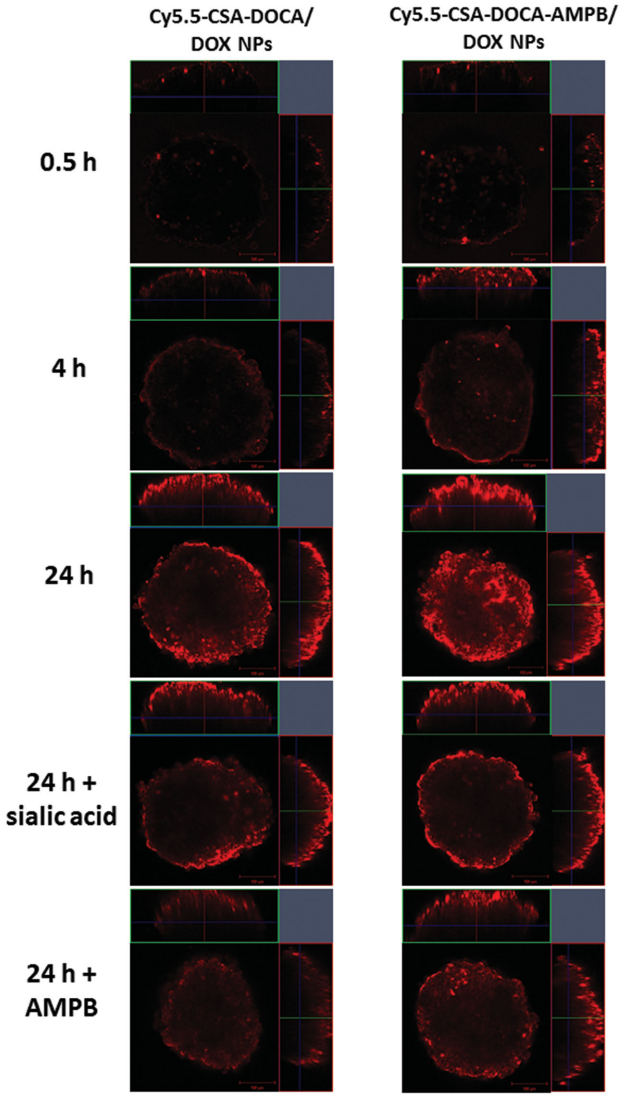

Figure 7. Uptake studies in A549 spheroid model. Penetration of Cy5.5-labeled NPs in A549 spheroids was observed by CLSM after incubating for 0.5, 4, and 24 h. Sialic acid (500×10^{-6} M) or AMPB (500×10^{-6} M) was pretreated at 24 h incubation group. The length of scale bar is 100 μm.

2.6. Tumor Penetration in a 3D Spheroid Model

The tumor penetration efficiency of the NPs was evaluated using an A549 tumor spheroid model and assessed using CLSM (**Figure 7** and Figure S5, Supporting Information). Amine-functionalized Cy5.5 was used as a fluorescence dye and conjugated to the carboxylic acid groups of CSA via amide bond formation. The distribution of Cy5.5-labeled CSA–DOCA/DOX NPs and CSA–DOCA–AMPB/DOX NPs in the spheroids was observed using CLSM. The Z-stacked images of the center of tumor spheroids treated with both NP groups are shown (Figure 7), and red fluorescence indicates the presence of NPs. The red fluorescence signal in the CSA–DOCA–AMPB NP-treated group is stronger than the CSA–DOCA NP-treated group (Figure 7). As shown in Figure S5 (Supporting Information), AMPB-conjugated NPs group exhibited a higher penetration efficiency into the core of tumor spheroids, compared to the AMPB-unmodified NPs group, after 0.5, 4, and 24 h of incubation ($p < 0.05$). Cotreatment of sialic acid or AMPB with CSA–DOCA–AMPB NPs significantly reduced the penetration of NPs into the spheroids ($p < 0.05$), comparable with that of the CSA–DOCA NPs group. Phenylboronic acid located in the surface of NPs can react with the sialic acid of cancer cells and form stable binding (Figure 1). It is known that complex of phenylboronic acid and sialic acid is based on intramolecular stabilization via a B—O bond.[12] Boronic acid-rich NPs have been shown to exhibit improved DOX penetration efficiency in 3D multicellular spheroid (MCS) models.[10] Formation of a complex of boronic acid and sialic acid can be a driving force for the movement of NPs from the periphery of tumors to the intermediate region, and ultimately to the necrotic core region. Homogeneous intratumoral distribution of drugs and macromolecules has been recognized as a key requirement of efficient cancer therapy and is limited by the elevated interstitial pressure in tumors.[9] The interaction between boronic acid and sialic acid can overcome this interstitial pressure and accomplish more homogeneous distribution of drug and NPs. It is important to note that the penetration of drug-loaded NPs to the core region of tumor tissue can inhibit tumor growth more efficiently than drug delivery to more peripheral areas of the tumor.

2.7. In Vitro Antitumor Efficacy in an A549 Multicellular Spheroid (MCS) Model

The in vitro antitumor efficacy and enhancement of tumor penetration of the NPs was assessed using an A549 MCS model. The spheroid model aims to reflect the characteristics of a tumor mass, and therefore it is regarded as a more efficient model for evaluating cellular uptake and cytotoxicity than 2D-cultured cells.[29] As shown in **Figure 8**, tumor growth suppression was observed in MCSs that had been treated with DOX solution or NPs while the tumor mass of the control group (no treatment) increased constantly. After culturing for 4 days, the tumor volume in the various groups decreased in the following order of effectiveness; control, DOX solution, CSA–DOCA/DOX NPs, and CSA–DOCA–AMPB/DOX NPs ($p < 0.05$). The addition of sialic acid or AMPB into both CSA–DOCA/DOX NPs and CSA–DOCA–AMPB/DOX NPs groups produced similar antitumor efficacy with the CSA–DOCA/DOX NPs group. It also indicated that the improved antitumor efficacy of AMPB-modified NPs, compared to the unmodified NPs, was based on the interaction between phenylboronic acid and sialic acid. On day 4, the tumor volume of the control group was 4.34-fold higher than that at the start of the experiment. On the contrary, the tumor volume in the CSA–DOCA–AMPB/DOX NP-treated group on day 4 was reduced to 44.7% of its initial size. Treatment with DOX solution also resulted in a relative tumor growth suppression effect, and tumor volume increased by only 10.6% after 4 d. In agreement with the results of the cellular uptake and cytotoxicity studies (Figure 6 and Figures S3 and S4, Supporting Information),

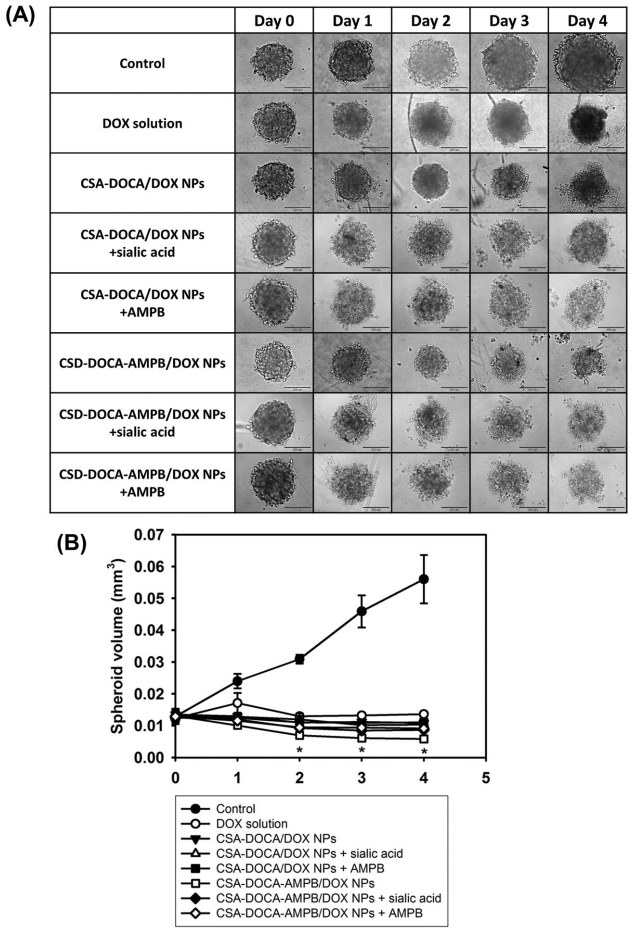

Figure 8. In vitro antitumor efficacy tests in A549 spheroid model. A) In vitro antitumor efficacy in A549 spheroid model was evaluated. The optical images of spheroids according to the incubation time were observed. The length of scale bar is 200 μm. B) The growth profiles of A549 spheroid for 4 days are shown. $^{*}p < 0.05$, compared to the other groups.

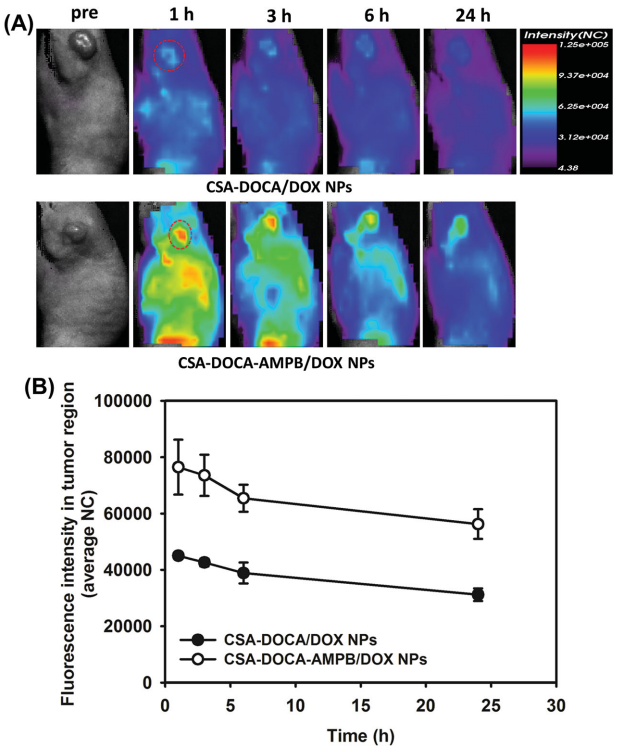

Figure 9. In vivo NIRF imaging study in A549 tumor-xenografted mouse model. Cy5.5-labeled CSA–DOCA/DOX NPs and CSA–DOCA–AMPB/DOX NPs were injected via tail vein. Real-time images were taken at 0 (pre), 1, 3, 6, and 24 h. A) Scanned images of whole body are presented. Red dashed circle indicates tumor region. B) Profiles of fluorescence intensity in tumor region (photon counts per mm^2), according to the time, are shown. Each point represents the mean ± SD ($n = 3$).

treatment with DOX-loaded NPs resulted in a larger inhibitory effect of tumor growth than treatment with DOX solution. It is interesting to note that the tumor volume in the CSA–DOCA–AMPB/DOX NP-treated group was 53.7%, compared to the CSA–DOCA/DOX NP-treated group on day 4 ($p < 0.05$). The results of the in vitro antitumor efficacy experiments using A549 MCS model can also be explained by the increased tumor penetration of AMPB-modified NPs (Figure 7 and Figure S5, Supporting Information). It can also be explained by the receptor-mediated endocytosis mechanisms allowed by the CSA–CD44 receptor and phenylboronic acid–sialic acid interactions.

2.8. Near-Infrared Fluorescence (NIRF) Imaging

The in vivo fate of the DOX-loaded NPs was monitored using NIRF imaging (**Figures 9–11**). Cy5.5 was used as a NIRF dye and conjugated to the CSA backbone via formation of an amide bond. Using an A549 tumor-xenografted mouse model, Cy5.5-labeled NPs were injected intravenously, and whole body images were scanned over 24 h (Figure 9). As shown in Figure 9A, the fluorescence intensity in the tumor region of the CSA–DOCA–AMPB/DOX NP-treated group was significantly stronger than that in the CSA–DOCA/DOX NP-treated group during the experiment. As time went by, the NPs in normal tissues and organs appeared to be excreted, and those in tumor region showed a relative increase after 24 h. The fluorescence intensity in the CSA–DOCA–AMPB/DOX NP-treated group was 80% higher than that in the group treated with unmodified NPs (Figure 9B). The biodistribution of the NPs in A549 tumor-xenografted mice was assessed using ex vivo NIRF imaging (Figure 10). Several organs and tissues, including the tumor, were dissected 24 h after injection, and Cy5.5-filtered images were recorded (Figure 10A). In the CSA–DOCA/DOX NP-treated group, the highest fluorescence signal was detected in the tumor, and considerable intensity was observed in the liver (Figure 10B). The fluorescence intensity in the CSA–DOCA–AMPB/DOX NP-treated group was very strong in the tumor region compared to other tissues and organs. A significant difference in fluorescence signal was shown between the tumor regions of both NP-treated groups ($p < 0.05$). A greater accumulation of NPs in the tumors of the CSA–DOCA–AMPB NP-treated group than the CSA–DOCA NP-treated group implies that AMPB modification increases tumor targeting. With primary tumor targeting based on the interaction between CSA and CD44 receptor, the specificity of

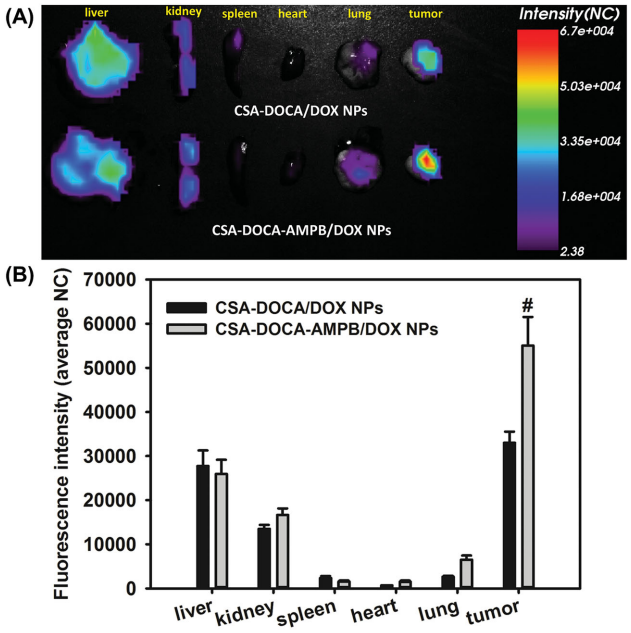

Figure 10. Biodistribution study of Cy5.5-labeled NPs in A549 tumor-xenografted mouse model by ex vivo NIRF imaging. At 24 h postinjection of Cy5.5-labeled CSA–DOCA/DOX NPs and CSA–DOCA–AMPB/DOX NPs, several tissues and organs were dissected and their fluorescence intensities were measured. A) NIRF image of dissected organs and tissues in both groups is presented. B) Fluorescence intensity in each organ or tissue was quantitatively analyzed and compared to each other. Each point represents the mean ± SD ($n = 3$). $^{\#}p < 0.05$, compared to CSA–DOCA/DOX NPs group.

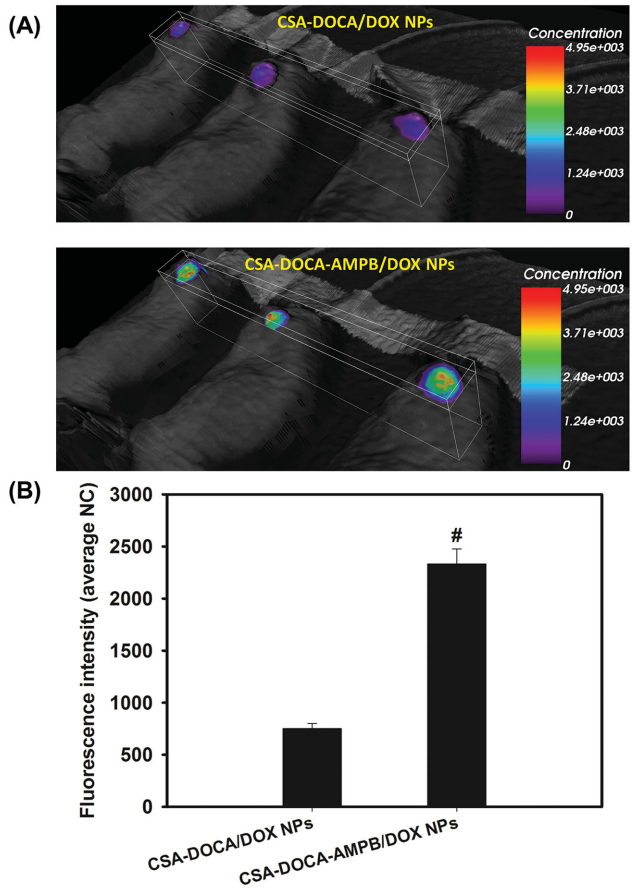

Figure 11. Tumor penetration assay observed by in vivo NIRF imaging. Cy5.5-labeled CSA–DOCA/DOX NPs and CSA–DOCA–AMPB/DOX NPs were injected intravenously to A549 tumor-xenografted mouse model. A) Z-stack images of tumor tissues at 24 h postinjection are presented. B) Quantitative analyzed fluorescence intensity in tumor tissue of both groups is shown. Data represents the mean ± SD ($n = 3$). $^{\#}p < 0.05$, compared to CSA–DOCA/DOX NPs group.

tumor targeting increases by the complex formation between boronic acid and sialic acid. The suitability of the NPs for passive tumor targeting via the EPR effect (i.e., ≈200 nm mean diameter) also contributed to their successful distribution to the tumors. This increased accumulation in tumors, and the reduced distribution to other tissues and organs would be expected to increase therapeutic efficacy and alleviate unwanted side effects.

The in vivo tumor penetration efficiency of the AMPB-modified NPs was evaluated using NIRF imaging with 3D analysis (Figure 11). Z-stack images of the tumor mass were acquired, and the NIRF intensity was compared in both NP-treated groups. The fluorescence intensity of the tumor in the CSA–DOCA–AMPB/DOX NP-treated group was 3.1-fold higher than that in the CSA–DOCA/DOX NP-treated group ($p < 0.05$). The relative ratio of fluorescence intensity in tumor site obtained by 3D analysis (Figure 11) was higher than that in the 2D experiment (Figures 9 and 10). This implies efficient movement of the AMPB-modified NPs from the tumor periphery to the tumor core. Because of the high interstitial pressure in solid tumors, simply arriving on the surface of the tumor is not sufficient for NPs to exert a therapeutic effect. Homogeneous distribution of NPs in tumor mass is necessary to completely inhibit tumor growth. The improved intracellular uptake and tumor penetration efficiency of AMPB-modified NPs observed in A549 cells and MCSs (Figures 6 and 7), respectively, correlates well with the results of the in vivo 3D NIRF imaging (Figure 11).

2.9. In Vivo Antitumor Efficacy

The in vivo antitumor efficacy of the NPs was assessed using an A549 tumor-xenografted mouse model (**Figure 12**). DOX solution, CSA–DOCA/DOX NPs, and CSA–DOCA–AMPB/DOX NPs were intravenously injected into the mouse five times. Tumor growth and body weight were then monitored for 24 days (Figure 12). The tumor volume in the CSA–DOCA–AMPB/DOX NP-treated group was significantly smaller than that in the other groups ($p < 0.05$). Although the mean value of body weight in DOX solution-treated group was slightly lower than that in the other groups, there was no significant difference between the NP-treated groups and control group. This indicates the improved safety of the NPs compared to treatment with DOX alone. The tumor growth inhibition effect that was exerted by AMPB-modified NPs can be explained by their excellent in vivo tumor targeting and penetration capabilities (Figures 9–11). Additionally, the sustained drug release pattern and increased tumor penetration efficiency observed for the CSA–DOCA–AMPB/DOX NPs,

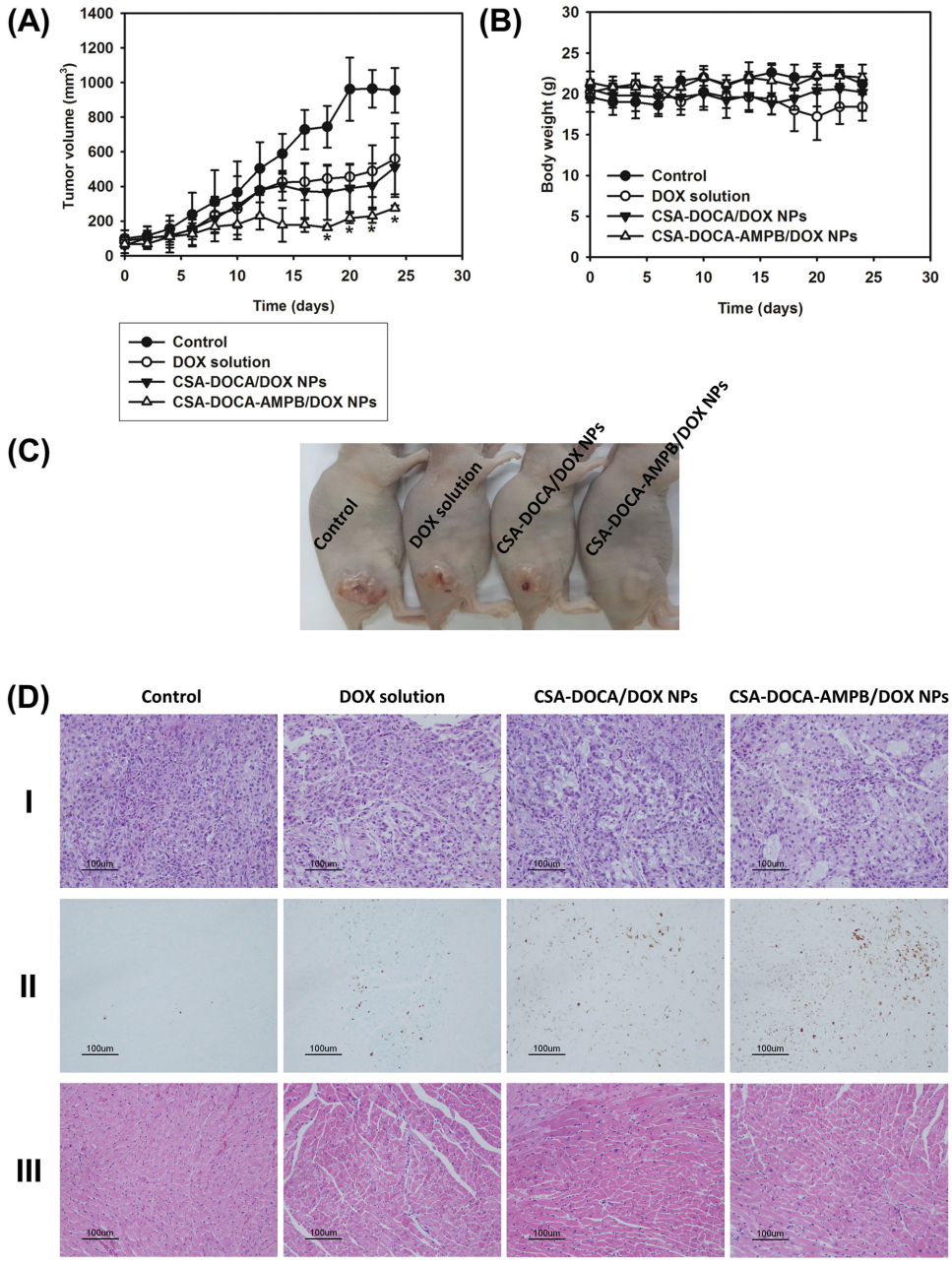

Figure 12. In vivo antitumor efficacy test in A549 tumor-xenografted mouse model. A) Tumor volume (mm^3) profiles according to time (days) are presented. DOX solution, CSA–DOCA/DOX NPs, and CSA–DOCA–AMPB/DOX NPs were injected intravenously on day 12, 14, 16, 18, and 20. B) Body weight (g) was monitored with tumor size for 24 days. C) Image of tumor in each group on day 24 is exhibited. Data represent mean ± SD ($n = 4$). $^{*}p < 0.05$, compared to the other groups. D) Histological assays of dissected tumor and heart. Tumor and heart were dissected from mice on day 24 after treatment with DOX solution, CSA–DOCA/DOX NPs, and CSA–DOCA–AMPB/DOX NPs. H&E staining of tumor (I) and heart (III) and TUNEL assay of tumor (II) were done and their microscopic images are presented.

compared to the AMPB-unmodified NPs, in the spheroid model also contributed to their improved tumor growth inhibition. Increased apoptosis in the tumor and reduced cardiac toxicity in the AMPB-modified NP-treated group were revealed by a terminal deoxynucleotidyl transferase dUTP nick end labeling (TUNEL) assay of the dissected tumor and hematoxylin and eosin (H&E) staining of the dissected heart (Figure 12D). Passive tumor targeting enabled by the EPR effect, active tumor targeting enabled by the interaction between CSA and CD44 receptor, improved tumor penetration caused by complex formation between boronic acid and sialic acid, and the improved biocompatibility of CSA–DOCA–AMPB-based NPs make them a promising nanosystem for cancer therapy and diagnosis.

3. Conclusion

Phenylboronic acid-rich, self-assembled NPs based on CSA–DOCA were fabricated to selectively deliver DOX to tumors. AMPB was attached to the CSA–DOCA conjugate and DOX-loaded NPs made from CSA–DOCA–AMPB with 206 nm mean diameter, narrow size distribution, negative zeta potential, and high drug encapsulation efficiency were prepared. DOX release from CSA–DOCA–AMPB NPs was higher at acidic pH (pH 5.5 and 6.8) than that at physiological pH (pH 7.4). CSA–DOCA–AMPB NPs exhibited improved cellular uptake in A549 cells and tumor penetration in A549 spheroids compared to CSA–DOCA NPs due to the interaction with sialic acid in the tumor tissue. In vivo tumor targeting based on the interaction between CSA and CD44 receptor was observed in A549 tumor-xenografted mice, and penetration of NPs into the core region of tumor mass was observed using NIRF imaging. Tumor targeting and penetration with CSA–DOCA–AMPB NPs were evidenced by improved tumor growth inhibition in a tumor-xenografted mouse model. These findings reveal that CSA–DOCA–AMPB NPs that can interact with both CD44 receptors and sialic acid may be a promising nanosystem for cancer theranosis.

4. Experimental Section

Materials: CSA (37 kDa average molecular weight), DOCA, AMPB, EDC, NHS, triethylamine (TEA), agarose, and deuterium oxide (D_2O) were purchased from Sigma-Aldrich Co. (St. Louis, MO, USA). DOX HCl was obtained from Boryung Pharmaceutical Co., Ltd. (Seoul, Korea). The NIRF dye, FCR-675 amine (Cy5.5-amine), was purchased from BioActs (DKC Corp., Incheon, Korea). Dimethyl sulfoxide-d_6 (DMSO-d_6) was purchased from Cambridge Isotope Laboratories, Inc. (Andover, MA, USA). DMSO was bought from Daejung Chemicals & Metals Co., Ltd. (Seoul, Korea). RPMI 1640 cell culture medium, penicillin, streptomycin, and fetal bovine serum (FBS) were obtained from Gibco Life Technologies, Inc. (Carlsbad, CA, USA). All other reagents were of analytical grade.

Synthesis and Characterization of CSA–DOCA–AMPB: DOCA-conjugated CSA (CSA–DOCA) was synthesized through amide bond formation. DOCA was modified with ethylenediamine to form EtDOCA to allow further reaction with the carboxylic acid group of CSA. Briefly, DOCA (1.177 g) was dissolved in methanol (MeOH; 5 mL), into which hydrochloric acid (184 µL) was added. The mixture was stirred and refluxed for 6 h at 60 °C, followed by concentration on a rotary evaporator and complete drying under vacuum. The resulting white powder was washed with ice-cold water and lyophilized to obtain methyldeoxycholate (DOCA-OMe). Then, DOCA-OMe was dissolved in ethylenediamine (50 molar equivalents). The solution was stirred for 8 h at 120 °C under reflux, before being cooled down to room temperature. The mixture was precipitated with water and filtered. The filtrate, EtDOCA, was further washed with an excess amount of water three times and freeze-dried. Subsequently, CSA was hydrophobically modified with EtDOCA to produce amphiphilic CSA–DOCA. In brief, CSA (100 mg) was dissolved in formamide (20 mL) at 80 °C and cooled down to room temperature. EDC (36.8 mg) and NHS (61.3 mg) were added to the CSA solution. The mixture was stirred for 20 min at room temperature to activate the carboxylic acid groups of CSA. Then, EtDOCA (34.8 mg) dissolved in dimethylformamide (DMF; 20 mL) was slowly added to the CSA solution. The reaction mixture was stirred for 20 h at room temperature, dialyzed against a mixture of water and methanol (25%–100%, v/v) for 3 days, and lyophilized. The resulting white powder, CSA–DOCA, was stored at 2–8 °C for further experiments. CSA–DOCA–AMPB was synthesized by attaching AMPB to CSA–DOCA. CSA–DOCA (100 mg) was dissolved in a mixture of DMSO and water (20 mL; 3:1, v/v). EDC (23.0 mg) and NHS (13.8 mg) were added, and the mixture was stirred for 20 min to activate the carboxylic acid groups of CSA–DOCA. Meanwhile, AMPB (7.5 mg) was dissolved in a mixture of DMSO and water (20 mL; 3:1, v/v) and added slowly to the activated CSA–DOCA solution. The reaction mixture was stirred for 20 h at room temperature, dialyzed against water for 2 days, and lyophilized. The resulting white powder, CSA–DOCA–AMPB, was stored at 2–8 °C for further use. For the evaluation of AMPB content in CSA–DOCA–AMPB, ^{1}H-NMR (Varian FT-500 MHz; Varian, Inc., Palo Alto, CA, USA) was used. CSA–DOCA, AMPB, and CSA–DOCA–AMPB were dissolved in a mixture of DMSO-d_6 and D_2O (3:1, v/v) for ^{1}H-NMR analysis.

Preparation and Characterization of DOX-Loaded NPs: DOX base was used as a model hydrophobic drug in this investigation. As previously reported,[19] DOX base was prepared by dissolving DOX HCl (100 mg) in DMSO (10 mL) with TEA (0.12 mL). After 12 h of stirring at room temperature, the solution was lyophilized and dried. To prepare DOX-loaded CSA–DOCA and CSA–DOCA–AMPB NPs, DOX (1 mg) and each polymer (7.5 mg) were dissolved in a mixture of DMSO and water (1 mL; 1:1, v/v), and the solvent was evaporated under an N_2 gas stream for 5 h at 70 °C. The drug and polymer composite film was resuspended in distilled water (DW; 1 mL) and filtered through a syringe filter (0.45 µm pore size; Minisart RC 15, Sartorius Stedim Biotech GmbH, Goettingen, Germany). To measure the encapsulation efficiency of DOX, the dispersion of NPs was disrupted with DMSO (50 times volume), and the drug content was analyzed using high-performance liquid chromatography (HPLC) system (Waters Co., Milford, MA, USA). It was equipped with a reverse phase C18 column (Xbridge RP18, 250 × 4.6 mm, 5 µm; Waters Co.), a separation module (Waters e2695), and fluorescence detector (Waters 2475). The mobile phase was composed of 10×10^{-3} M potassium phosphate buffer (pH 2.5, adjusted with phosphoric acid) and acetonitrile with 0.1% TEA (71:29, v/v), and the flow rate was set to 1.0 mL min^{-1}. The injection volume was 20 µL, and the eluent was monitored at the excitation and emission wavelengths of 470 and 565 nm, respectively. The morphology of the DOX-loaded NPs was observed using TEM (JEM 1010; JEOL, Tokyo, Japan). The samples were stained with 2% (w/v) phosphotungstic acid solution, placed on the copper grid coated with carbon film, and dried at room temperature. The particle size, polydispersity index, and zeta potential of the NPs were measured using electrophoretic light scattering (ELS-Z; Otsuka Electronics, Tokyo, Japan) according to the manufacturer's protocol.

In Vitro Drug Release: The DOX release behavior from DOX-loaded CSA–DOCA and CSA–DOCA–AMPB NPs was evaluated. Aliquots (150 µL) of NPs dispersions were loaded into mini-GeBAflex tubes (14 kDa molecular weight cutoff; Gene Bio-Application Ltd., Kfar Hanagide, Israel). Each dialysis tube was immersed into phosphate-buffered saline (PBS; 10 mL; pH 7.4 for CSA–DOCA NPs, and pH 5.5, 6.8, or 7.4 for CSA–DOCA–AMPB NPs, adjusted with phosphoric acid) and agitated at 50 rpm at 37 °C. Aliquots (200 µL) of the release media were collected at predetermined times (1, 2, 4, 6, 8, 24, 48, 72, 96, and 120 h), and the same volume of fresh medium was replenished at each time point. The amount of drug released was determined using the above-mentioned HPLC method.

In Vitro Cytotoxicity: A549 cells (human lung adenocarcinoma cell; Korean Cell Line Bank, Seoul, Korea) were cultured in RPMI 1640, containing L-glutamine (300 mg L^{-1}), supplemented with 10% (v/v) heat inactivated FBS, 1% (v/v) penicillin (100 U mL^{-1}), and streptomycin (0.1 mg mL^{-1}). Cells were maintained in a 5% CO_2 atmosphere with 95% relative humidity at 37 °C and trypsinized at 70%–80% confluency for the following cellular uptake studies. The cytotoxicity of CSA–DOCA and CSA–DOCA–AMPB conjugates was evaluated using a [3-(4,5-dimethyl-2-yl)-5-(3-carboxymethoxyphenyl)-2-(4-sulfophenyl)-2H-tetrazolium, inner salt] (MTS) assay. A549 cells were seeded onto 96-well plates at a density of 1.0×10^4 cells per well and incubated with various concentrations (1, 2, 5, 10, 20, 50, 100, 200, and 500 µg mL^{-1}) of each conjugate. After incubating for 24, 48, or 72 h at 37 °C, the cells were treated with CellTiter 96 AQ_{ueous} One Solution Cell Proliferation

Assay Reagent (Promega Corp., Madison, WI, USA) and incubated for an additional 4 h at 37 °C according to the manufacturer's instructions. The absorbance was measured at a wavelength of 490 nm using a UV–vis spectrophotometer (EMax Precision Microplate Reader, Molecular Devices Corp., Sunnyvale, CA, USA).

Cellular Uptake in the Cell Culture Model: A549 cells were cultured using the same conditions as described previously. Cellular distribution of drug was assessed using CLSM. A549 cells were seeded on culture slides (BD Falcon, Bedford, MA, USA) at a density of 1.0×10^5 cells per well (surface area of 1.7 cm^2 per well, four-chamber slides) and incubated overnight at 37 °C. DOX solution or DOX-loaded NPs suspension (corresponding to 100×10^{-6} M DOX concentration) was added to the cells. To verify the interaction between AMPB and sialic acid, sialic acid (500×10^{-6} M) was preincubated with the NPs suspensions and added to the cells, and AMPB (500×10^{-6} M) was preincubated with the cells prior to adding NPs suspension to the cells, respectively. Cells were incubated for 1 h, washed with PBS (pH 7.4) three times, and fixed in 4% (v/v) formaldehyde solution for 10 min. They were then dried under an air stream, and VECTASHIELD mounting medium with 4′,6-diamidino-2-phenylindole (DAPI; H-1200, Vector laboratories, Inc., CA, USA) was added to the culture slides. Cells were observed using CLSM (LSM 710, Carl-Zeiss, Thornwood, NY, USA).

Tumor Penetration in a 3D Spheroid Model: For the preparation of MCSs, A549 cells, at a density of 500 cells per well, were seeded onto round-bottomed 96-well plates coated with a thin layer of agarose (2% [w/v] in Hank's balanced salt solution) and cultured in the same culture medium as described previously. The cells were incubated in 5% CO_2 atmosphere with 95% relative humidity at 37 °C with gentle agitation, and the culture medium was replaced every other day. A549 MCSs were harvested after 5–7 days when reaching a diameter of around 500 μm.[10] To evaluate the tumor penetration of CSA–DOCA and CSA–DOCA–AMPB NPs into MCSs, the NPs were labeled with Cy5.5, a NIRF probe, and their distribution within MCSs was observed using CLSM. Cy5.5-amine was conjugated to the carboxylic acid group of the CSA backbone via amide bond formation. CSA–DOCA (50 mg) or CSA–DOCA–AMPB (50 mg) was dissolved in a mixture of water and DMSO (25 mL; 1:1, v/v). EDC (168.1 mg) and NHS (20.5 mg) were added. After stirring at room temperature for 15 min, Cy5.5-amine (0.2 mg) dissolved in DMSO (0.2 mL) was slowly added, and the solution was stirred for 24 h. The resultant mixture was dialyzed against water for 2 days and then lyophilized. The MCSs were incubated with Cy5.5-labeled CSA–DOCA or CSA–DOCA–AMPB NPs at a concentration of 5 μg mL^{-1} for 0.5, 4, and 24 h. The Cy5.5 concentration was determined using a fluorescence spectrophotometer (SpectraMax M5 multimode microplate reader, Molecular Devices Corp.) at excitation and emission wavelengths of 675 and 700 nm, respectively. Sialic acid (500×10^{-6} M) or AMPB (500×10^{-6} M) was cotreated with CSA–DOCA NPs and CSA–DOCA–AMPB NPs groups. After incubating, MCSs were washed with PBS (pH 7.4) three times and fixed with 4% (v/v) formaldehyde solution for 10 min. The MCSs were then placed onto a coverslip bottom dish and observed using CLSM (LSM 710, Carl-Zeiss).

In Vitro Antitumor Efficacy Test Using an A549 MCS Model: To prepare A549 MCSs, cells were seeded onto round-bottomed 96-well plates, coated with a thin layer of agarose (2% [w/v] in Hank's balanced salt solution) at a density of 500 cells per well, and cultured in the same culture medium as described previously. They were incubated in 5% CO_2 atmosphere with 95% relative humidity at 37 °C with gentle agitation, and the culture medium was replaced every other day. When the diameter of MCS reached around 300 μm, DOX solution or DOX-loaded NPs (corresponding to 50 μg mL^{-1} DOX concentration) was added and incubated for 24 h. To demonstrate the interaction between AMPB and sialic acid, sialic acid (500×10^{-6} M) was preincubated with the NPs suspensions and added to the spheroids, and AMPB (500×10^{-6} M) was preincubated with the spheroids prior to adding NPs suspension to the spheroids, respectively. After removing the drug solution or drug-loaded NPs, fresh cell culture media was added and replaced every other day. Morphology of A549 MCS was observed using inverted fluorescence microscopy (IX70, Olympus, Tokyo, Japan) over 4 days. The volume (V, mm^3) of spheroid was calculated with the following formula: $V = 0.5 \times$ longest diameter $\times$ (shortest diameter)^2.

Real-Time NIRF Imaging: For the NIRF imaging study, Cy5.5-conjugated CSA–DOCA or CSA–DOCA–AMPB NPs were injected into A549 tumor-bearing mice and fluorescence intensities were scanned using an Optix MX3 (ART Advanced Research Technologies, Inc., Saint-Laurent, Canada). To prepare the A549 tumor-xenografted mouse model, female BALB/c nude mice (5-weeks-old, Charles River, Wilmington, MA, USA) were used. Mice were maintained in a light-controlled room kept at a temperature of 22 ± 2 °C with a relative humidity of 55% ± 5% (Animal Center for Pharmaceutical Research, College of Pharmacy, Seoul National University, Korea). The experimental protocols for the animal study were approved by the Animal Care and Use Committee of the College of Pharmacy, Seoul National University. A suspension of A549 cells (2×10^6 cells in 0.1 mL cell culture media) was injected into the back of the mice. NIRF imaging was performed on mice with a tumor volume of 150–200 mm^3. The tumor volume (V, mm^3) was calculated using the following formula: $V = 0.5 \times$ longest diameter $\times$ (shortest diameter)^2. Cy5.5-labeled CSA–DOCA or CSA–DOCA–AMPB NPs were injected into the tail vein of the mouse at a dose of 0.12 mg kg^{-1} (Cy5.5 amount per body weight). A laser diode with a wavelength of 670 nm was used for the excitation of Cy5.5. Fluorescence intensities were scanned at 1, 3, 6, and 24 h postinjection. The tumor-bearing mice were euthanized, and their organs (liver, kidneys, spleen, heart, and lungs) and tumors were dissected for ex vivo imaging to monitor the biodistribution of NPs. To compare the penetration and retention of NPs in tumor tissue, volumetric data were generated using OptiView 3D Reconstruction module (version 3.2; ART Advanced Research Technologies, Inc.), which can construct fluorescence intensity in 3D space from time-resolved fluorescence measurements. The fluorescence intensity of the region of interest (ROI) (i.e., the tumor tissue) was reconstructed three-dimensionally, and the penetration into the tumor tissue was estimated by comparing the sliced planes of the ROI.

In Vivo Antitumor Efficacy: To prepare the A549 tumor-bearing mouse model, female BALB/c nude mice (5-weeks-old, Charles River) were used. Mice were maintained in a light-controlled room kept at a temperature of 22 ± 2 °C with a relative humidity of 55% ± 5%. The experimental protocols used in these animal studies were also approved by the Animal Care and Use Committee of the College of Pharmacy, Seoul National University. An A549 cell suspension (2×10^6 cells in 0.1 mL cell culture media) was subcutaneously injected into the back of the mice. After the tumor volume reached 50–100 mm^3, tumor size and body weight were measured. The tumor volume (mm^3) was calculated as $V = 0.5 \times$ longest diameter $\times$ (shortest diameter)^2. The experimental groups were as follows: control, DOX solution-treated, CSA–DOCA/DOX NP-treated, and CSA–DOCA–AMPB/DOX NP-treated. DOX (at a dose of 5 mg kg^{-1} as DOX) was injected intravenously into each mouse on day 12, 14, 16, 18, and 20. The tumor volumes and body weights of the mice were measured for 24 days. The tumors and hearts were then dissected at the end of the test for histological staining. Those were fixed with 4% (v/v) formaldehyde for 1 day, and 6 μm sections were deparaffinized and hydrated with ethanol. The tumors and hearts were also stained with H&E according to the standard procedure. The apoptotic effect was evaluated by TUNEL assay. Chromogen diaminobenzene (DAB) was incubated for color development for detecting DNA fragmentation resulting from apoptotic signaling cascades.

Statistical Analysis: All experiments in this study were performed at least three times, and the data are represented as the mean ± standard deviation (SD). Statistical analyses were carried out using a two-tailed t-test or analysis of variance (ANOVA), and $p < 0.05$ was considered significantly different.

Supporting Information

Supporting Information is available from the Wiley Online Library or from the author.

Acknowledgements

This research was supported by the National Research Foundation of Korea (NRF), funded by the Korean government (MSIP) (Grant Nos. 2009-0083533 and NRF-2012R1A1A1038944). Prof. H. J. Cho and Prof. D. D. Kim are co-corresponders of this work.

Received: February 17, 2015
Revised: March 23, 2015
Published online: May 8, 2015

[1] J. Fang, H. Nakamura, H. Maeda, *Adv. Drug Delivery Rev.* **2011**, *63*, 136.
[2] F. Alexis, E. Pridgen, L. K. Molnar, O. C. Farokhzad, *Mol. Pharm.* **2008**, *5*, 505.
[3] H. J. Cho, H. Y. Yoon, H. Koo, S. H. Ko, J. S. Shim, J. H. Lee, K. Kim, I. C. Kwon, D. D. Kim, *Biomaterials* **2011**, *32*, 7181.
[4] O. C. Farokhzad, J. Cheng, B. A. Teply, I. Sherifi, S. Jon, P. W. Kantoff, J. P. Richie, R. Langer, *Proc. Natl. Acad. Sci. U.S.A.* **2006**, *103*, 6315.
[5] S. K. Sahoo, W. Ma, V. Labhasetwar, *Int. J. Cancer* **2004**, *112*, 335.
[6] S. Xuan, D. Shin, J.-S. Kim, *J. Pharm. Invest.* **2014**, *44*, 473.
[7] H. Holback, Y. Yeo, *Pharm. Res.* **2011**, *28*, 1819.
[8] C. H. Heldin, K. Rubin, K. Pietras, A. Ostman, *Nat. Rev. Cancer* **2004**, *4*, 806.
[9] A. B. Ariffin, P. F. Forde, S. Jahangeer, D. M. Soden, J. Hinchion, *Cancer Res.* **2014**, *74*, 2655.
[10] X. Wang, X. Zhen, J. Wang, J. Zhang, W. Wu, X. Jiang, *Biomaterials* **2013**, *34*, 4667.
[11] C. Bull, M. A. Stoel, M. H. den Brok, G. J. Adema, *Cancer Res.* **2014**, *74*, 3199.
[12] S. Deshayes, H. Cabral, T. Ishii, Y. Miura, S. Kobayashi, T. Yamashita, A. Matsumoto, Y. Miyahara, N. Nishiyama, K. Kataoka, *J. Am. Chem. Soc.* **2013**, *135*, 15501.
[13] A. Matsumoto, N. Sato, K. Kataoka, Y. Miyahara, *J. Am. Chem. Soc.* **2009**, *131*, 12022.
[14] J. Wang, Z. Zhang, X. Wang, W. Wu, X. Jiang, *J. Controlled Release* **2013**, *168*, 1.
[15] H. Liu, Y. Li, K. Sun, J. Fan, P. Zhang, J. Meng, S. Wang, L. Jiang, *J. Am. Chem. Soc.* **2013**, *135*, 7603.
[16] Y. S. Liu, C. C. Chiu, H. Y. Chen, S. H. Chen, L. F. Wang, *Mol. Pharmaceutics* **2014**, *11*, 1164.
[17] Y. J. Lin, Y. S. Liu, H. H. Yeh, T. L. Cheng, L. F. Wang, *Int. J. Nanomed.* **2012**, *7*, 4169.
[18] W. Park, S. J. Park, K. Na, *Colloids Surf., B* **2010**, *79*, 501.
[19] H. J. Cho, I. S. Yoon, H. Y. Yoon, H. Koo, Y. J. Jin, S. H. Ko, J. S. Shim, K. Kim, I. C. Kwon, D. D. Kim, *Biomaterials* **2012**, *33*, 1190.
[20] U. Termsarasab, H. J. Cho, D. H. Kim, S. Chong, S. J. Chung, C. K. Shim, H. T. Moon, D. D. Kim, *Int. J. Pharm.* **2013**, *441*, 373.
[21] P. Decuzzi, R. Pasqualini, W. Arap, M. Ferrari, *Pharm. Res.* **2009**, *26*, 235.
[22] Y. J. Jin, U. Termsarasab, S. H. Ko, J. S. Shim, S. Chong, S. J. Chung, C. K. Shim, H. J. Cho, D. D. Kim, *Pharm. Res.* **2012**, *29*, 3443.
[23] U. Termsarasab, I. S. Yoon, J. H. Park, H. T. Moon, H. J. Cho, D. D. Kim, *Int. J. Pharm.* **2014**, *464*, 127.
[24] S. Ganesh, A. K. Iyer, D. V. Morrissey, M. M. Amiji, *Biomaterials* **2013**, *34*, 3489.
[25] H. J. Cho, J. Oh, M. K. Choo, J. I. Ha, Y. Park, H. J. Maeng, *Int. J. Biol. Macromol.* **2014**, *63*, 15.
[26] J. Li, M. Huo, J. Wang, J. Zhou, J. M. Mohammad, Y. Zhang, Q. Zhu, A. Y. Waddad, Q. Zhang, *Biomaterials* **2012**, *33*, 2310.
[27] H. T. Moon, Y. K. Lee, J. K. Han, Y. Byun, *J. Biomater. Sci., Polym. Ed.* **2002**, *13*, 817.
[28] J. Xi, J. Qin, L. Fan, *Int. J. Nanomed.* **2012**, *7*, 5235.
[29] D. V. LaBarbera, B. G. Reid, B. H. Yoo, *Expert Opin. Drug Discovery* **2012**, *7*, 819.